Earth and Planetary Science Letters 269 (2008) 435–446

Contents lists available at ScienceDirect

Earth and Planetary Science Letters

journal homepage: www.elsevier.com/locate/epsl

Thinning of continental backarc lithosphere by flow-induced gravitational instability

Claire A. Currie [a,b,*], Ritske S. Huismans [a,c], Christopher Beaumont [a]

[a] Department of Oceanography, Dalhousie University, Halifax, NS, Canada B3H 4J1
[b] Department of Physics, University of Alberta, Edmonton, AB, Canada T6G 2G7
[c] Department of Earth Science, Bergen University,Allegaten 41, N-5007, Bergen, Norway

ARTICLE INFO

Article history:
Received 1 February 2007
Received in revised form 19 January 2008
Accepted 24 February 2008
Available online 7 March 2008

Editor: C.P. Jaupart

Keywords:
subduction zone
mantle lithosphere
gravitational instability
thermal–mechanical model
Cascadia subduction zone
Canadian Cordillera

ABSTRACT

Many continental backarcs have thin (~60 km) lithosphere for 100s of km behind the volcanic arc, even where there has been no significant extension. One mechanism to produce thin backarc lithosphere is through gravitational thinning of normal thickness lithosphere by subduction-related mantle flow. The stability of backarc mantle lithosphere is examined using thermal–mechanical models of subduction of an oceanic plate beneath continental lithosphere with an initial thickness of 120 km and a thermal structure similar to average Phanerozoic continental lithosphere. Subduction-induced mantle flow shears the base of the backarc lithosphere, producing lateral density perturbations. Owing to the non-Newtonian lithosphere rheology, shearing also reduces the effective viscosity of the lowermost lithosphere, enabling the density perturbations to become gravitationally unstable. The perturbations develop into rapidly-growing downwellings which result in removal of lower backarc lithosphere on timescales of 5–10 Ma. Conductive heating and shearing of the remaining lithosphere results in a second, more muted, phase of gravitational instability and thinning. Lower lithosphere instability is enhanced by higher subduction rates, weaker intrinsic rheology, higher compositional density, and hotter initial thermal structure. The numerical model results are in good agreement with a buoyancy stability analysis, which includes the vertical gradients in temperature and strain rate through the lithosphere. As both rheology and density depend on lithosphere composition, significant thinning may be restricted to continental mantle lithosphere that is fertile and contains a small amount of water. To produce a final thickness comparable to that observed without lithospheric contraction or extension, it is necessary to have a weak lithosphere rheology, an initial thermal structure hotter than average Phanerozoic continental geotherms, or a combination of the two. The region of thin lithosphere at the northern Cascadia backarc coincides with terranes that were accreted to the North American craton. The known fertile composition of the backarc lithosphere may allow it to be thinned, while the drier, more refractory craton lithosphere is resistant to thinning.

1. Introduction

Some of the thinnest continental lithosphere is found in the backarc of subduction zones. Currie and Hyndman (2006) compiled observational constraints on lithosphere thermal structure for circum-Pacific continental backarcs that have not experienced significant recent extension. In most cases, high temperatures in the crust and shallow mantle are found for several hundred kilometers behind the volcanic arc and indicate a 60–70 km lithosphere thickness, approximately half the average thickness of Phanerozoic continental lithosphere (e.g. Poudjom et al., 2001). As an example, Fig. 1 shows thermal constraints for the northern Cascadia backarc. Indicators of high backarc temperatures include: 1) surface heat flow of 75 mW/m^2 (Fig. 1a), 2) low mantle seismic velocities (Fig. 1b), 3) estimates of high temperatures from peridotite xenolith thermobarometry, 4) present-day widespread sporadic basaltic volcanism, 5) high elevations (1.5–2 km) for a ~35 km backarc crustal thickness, and 6) an effective elastic thickness less than 30 km (Currie and Hyndman, 2006 and references therein). Together, the observations are consistent with a temperature of 1200 °C at ~60 km depth and a lithosphere thickness only slightly larger (Currie and Hyndman, 2006). The eastern limit of high temperatures and thin lithosphere coincides with the Rocky Mountain Trench, 500 km east of the volcanic arc, based on rapid changes in lithosphere properties and deformation style (Lowe and Ranalli, 1993; Hyndman and Lewis, 1999).

The origin of thin lithosphere in subduction zone backarcs is not well-understood. It is possible that the thin lithosphere is not related to subduction, for example, it is inherited from pre-subduction tectonics or due to the proximity of a mantle plume. On the other hand, subduction itself may trigger lithospheric thinning. One mechanism for producing thin lithosphere is through widespread backarc extension. The over-riding plate may also be thinned through ablative subduction, where lithosphere is mechanically removed by viscous drag from the subducting plate (Tao and O'Connell, 1992).

* Corresponding author. Department of Physics, University of Alberta, Edmonton, AB, Canada, T6L 2G7. Tel.: +1 780 492 1062; fax: +1 780 492 0714.
E-mail address: ccurrie@phys.ualberta.ca (C.A. Currie).

0012-821X/$ – see front matter © 2008 Elsevier B.V. All rights reserved.
doi:10.1016/j.epsl.2008.02.037

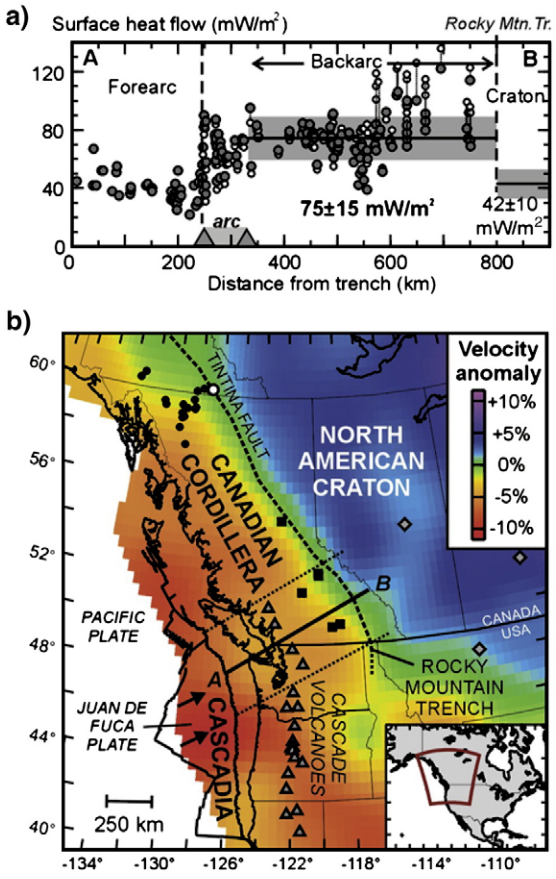

Fig. 1. a) Surface heat flow profile for the northern Cascadia subduction zone. The observed data (open circles) have been corrected for variations in upper crustal radioactive heat production (solid circles) (Currie and Hyndman, 2006). b) S-wave velocity anomalies at 100 km depth for the Cascadia subduction zone and Canadian Cordillera (van der Lee and Frederiksen, 2005). Line A–B is the heat flow profile; dotted lines denote the data swath width. Grey triangles are active arc volcanoes. Black squares are Cordilleran mantle xenolith sites (Peslier et al., 2000). Circles are locations of alkaline basalt centers; white circle is the Watson Lake site (Monger and Price, 2002). Grey diamonds are craton mantle xenolith sites (Griffin et al., 2004).

Another possibility is that fluids released from the subducting plate may infiltrate the overlying lithosphere, weakening it and making it susceptible to thinning by gravitational instability and flow in the underlying mantle. (Arcay et al., 2005, 2006) showed that hydrous weakening could lead to thinned lithosphere over a ~200 km width in the volcanic arc region, as most water is driven from the subducting plate at shallow depths. It is difficult to explain observations of thin lithosphere hundreds of kilometers behind the arc with this mechanism, unless slab-derived water can be carried far into the backarc, perhaps by transport in the convecting mantle or during earlier flat slab subduction (e.g. Dixon et al., 2004).

In this study, we investigate the idea that wide regions of thin backarc lithosphere may result from gravitationally-driven thinning of normal thickness lithosphere. Owing to its lower temperature, mantle lithosphere may be more dense than sublithospheric mantle and thus may be prone to gravitational instability, where the lower part of the lithosphere is removed through Rayleigh–Taylor-type downwelling. This differs from continental delamination (Bird, 1979) in that only the lowermost lithosphere participates in the instability, whereas delamination involves the peeling of the entire mantle lithosphere from the crust.

One way in which instability may be induced is through mechanical thickening of the lithosphere during horizontal shortening (Houseman et al., 1981). This process has been invoked to explain evidence of recent (<10 Ma) lithosphere thinning from seismic tomography data, volcanism, and changes in surface elevation in parts of the Central Andes backarc, which has undergone 300–350 km of shortening since the mid-Tertiary (Kay and Kay, 1993; Allmendinger et al., 1997; Garzione et al., 2006). This mechanism has also been proposed for parts of the northern Cascadia backarc (Ranalli et al., 1989). Conversely, gravitational instability may be initiated by subduction-related flow in the underlying mantle. This is the focus of the current study.

We use numerical thermal–mechanical models to investigate subduction of an oceanic plate beneath a continental plate. Through numerical experiments, we examine the conditions under which continental backarc lithosphere may undergo gravitational instability and thinning. We first study the relationship between mantle lithosphere stability and its intrinsic rheology and density structure, which are related to composition. We then investigate how subduction rate and thermal structure affect lithosphere stability.

2. Numerical model description

The initial geometry of the two-dimensional numerical models is shown in Fig. 2. The model domain has a width of 2000 km and depth of 660 km. The oceanic plate is composed of oceanic crust and mantle lithosphere, with a total thickness of 90 km. The continental plate has an initial thickness of 120 km, consisting of a 24 km upper-mid continental crust, 12 km lower crust, and 84 km mantle lithosphere. Backarc lithosphere stability is studied through numerical experiments in which material properties are varied in a ~800 km wide block of continental mantle lithosphere closest to the subduction zone (the backarc). Convergence between the two plates is kinematically imposed along the left-hand (seaward) model boundary. Within the model domain, the dynamics are driven by the far-field velocity boundary conditions and by buoyancy forces associated with thermal and compositional density variations.

2.1. Governing equations

Arbitrary Lagrangian–Euleran (ALE) finite element techniques are used to solve for plane strain deformation of viscous-plastic materials and the associated thermal field (Fullsack, 1995). Creeping flow is governed by the quasi-static force balance and conservation of mass equations, assuming incompressibility and zero Reynolds number:

$$\frac{\partial v_j}{\partial x_j} = 0 \tag{1}$$

$$\frac{\partial \sigma_{ij}}{\partial x_i} + \rho g = 0 \quad j = 1,2 \tag{2}$$

where $x_{i,j}$ are spatial coordinates, v_j are velocity components, ρ is density, and g is (vertical) gravitational acceleration. Repeated indices imply summation. The associated stress tensor is:

$$\sigma_{ij} = -P\delta_{ij} + \sigma'_{ij} = -P\delta_{ij} + 2\eta_{\mathrm{eff}}\dot{\varepsilon}_{ij} \tag{3}$$

where P is pressure (mean stress), σ'_{ij} is the deviatoric stress tensor, η_{eff} is the effective viscosity, δ_{ij} is the Kronecker delta ($\delta_{ij}=1$ for $i=j$; 0 otherwise), and the strain rate tensor is:

$$\dot{\varepsilon}_{ij} = \frac{1}{2}\left(\frac{\partial v_i}{\partial x_j} + \frac{\partial v_j}{\partial x_i}\right) \tag{4}$$

The two-dimensional thermal structure is governed by the energy balance equation:

$$\rho c_{\mathrm{p}}\left(\frac{\partial T_{\mathrm{K}}}{\partial t} + v_i\frac{\partial T_{\mathrm{K}}}{\partial x_i}\right) = k\frac{\partial}{\partial x_i}\frac{\partial T_{\mathrm{K}}}{\partial x_i} + A + v_z\alpha g T\rho \tag{5}$$

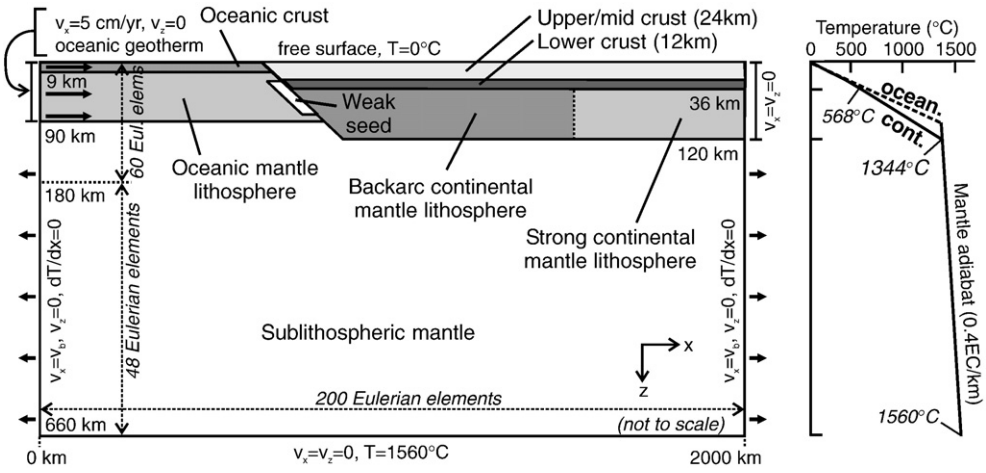

Fig. 2. Initial geometry and boundary conditions of the numerical models. The Eulerian mesh consists of 200 elements in the horizontal direction and 108 elements in the vertical direction, with refinement in the upper 180 km. The thermal structure of the oceanic and continental regions at the time of subduction initiation is shown on the right.

where T_K is absolute temperature, t is time, c_p is specific heat, k is thermal conductivity, A is volumetric radioactive heat production, v_z is vertical velocity, and α is the thermal expansion coefficient. The last term is the temperature correction for adiabatic heating or cooling.

Mechanical and thermal calculations are carried out on an Eulerian mesh that stretches vertically to conform to the upper surface of the model. Mechanical and thermal material properties are tracked on a Lagrangian mesh and additional Lagrangian tracer/tracking particles which are advected with the model velocity field (Fullsack, 1995). The numerical accuracy of the finite element code and mesh size has been verified through benchmarking against analytic and numerical studies of Rayleigh–Taylor and convective instabilities (Houseman and Molnar, 1997; Molnar et al., 1998).

2.2. Rheology, density and thermal parameters

All materials have a viscous-plastic rheology. When the deviatoric stress is below frictional-plastic yield, flow is viscous, with an effective viscosity (η^v_{eff}):

$$\eta^v_{\text{eff}} = f(B^*)\left(\dot{I}'_2\right)^{(1-n)/2n} \exp\left(\frac{Q+PV^*}{nRT_K}\right) \quad (6)$$

where f is a scaling factor (see below, $\dot{I}'_2$ is the second invariant of the strain rate tensor $\left(\dot{I}'_2 = \frac{1}{2}\dot{\varepsilon}_{ij}\cdot\dot{\varepsilon}_{ij}\right)$, R is the gas constant, and B*, n, Q and V* are the pre-exponential viscosity parameter, stress exponent, activation energy and activation volume from laboratory data. The parameter B* includes a conversion from the uniaxial laboratory experiments to the plane strain numerical models.

Frictional-plastic (brittle) deformation is defined by a Drucker–Prager yield criterion, equivalent to the Coulomb yield criterion in plane strain (Fullsack, 1995). The plastic yield stress is:

$$(J'_2)^{\frac{1}{2}} = c_0 + P\sin\phi_{\text{eff}} \quad (7)$$

where J'_2 is the second invariant of the deviatoric stress tensor $\left(J'_2 = \frac{1}{2}\sigma'_{ij}\sigma'_{ij}\right)$· c_0 is the cohesion, ϕ_{eff} is the effective internal angle of friction, which includes the effects of pore fluid pressure (e.g. Beaumont et al., 2006). Plastic deformation is modeled by defining an effective viscosity that places the state of stress on yield (Fullsack, 1995; Willett, 1999).

The rheological parameters used in the numerical models are given in Table 1a. Plastic materials strain soften over a prescribed range of accumulated strain, as an approximation of material weakening or increase in pore fluid pressure (reduction in ϕ_{eff}) with increasing strain (e.g. Huismans and Beaumont, 2003). Viscous deformation is calculated using laboratory-derived flow laws. The application of the flow laws to nature is subject to considerable uncertainty, primarily due to variability in composition and volatile content of natural rocks and uncertainties in the extrapolation of laboratory data to geological conditions. Given these uncertainties, the models are based on a reference set of flow laws and a scaling factor (f) is used to linearly scale the effective viscosity relative to the laboratory results (Eq. (6)). This approach allows for an assessment of model sensitivity to reasonable variations in viscous strength without invoking additional flow laws, each with their own uncertainties (Beaumont et al., 2006).

Laboratory data show that water and other volatiles decrease the viscous strength of the mantle; water-saturated olivine is 5–20 times weaker than dehydrated olivine at the same strain rate (Karato and Wu, 1993; Hirth and Kohlstedt, 1996; Hirth and Kohlstedt, 2003; Karato, 2003). In the models, the rheologies of the mantle lithosphere and sublithospheric mantle are based on wet olivine dislocation creep (Karato, 2003), and the scaling factor is used to approximate the effect of variations in volatile content. Higher values of f represent drier, stronger mantle. The scaling factor can also be interpreted to reflect changes in strength due to minor compositional variations.

For the sublithospheric mantle, $f=1$. At reasonable strain rates (10^{-15} to 10^{-16} s^{-1}), this gives an effective viscosity of ~10^{19} Pa s for the shallow upper mantle, similar to that inferred below non-cratonic regions (Cadek and Fleitout, 2003). The oceanic mantle lithosphere has $f=10$, corresponding to strengthening due to melt extraction and dehydration during lithosphere formation (e.g. Hirth and Kohlstedt, 1996). Landward of the backarc lithosphere block, the continental mantle lithosphere also has $f=10$. This region represents a water-poor, refractory continental interior, although it is not a craton in terms of its density or thermal structure. In the reference model, $f=1$ for the backarc mantle lithosphere. As discussed below, this represents a fertile mantle lithosphere containing a small amount of volatiles.

The lower continental crust and oceanic crust have a dry Maryland diabase rheology (Mackwell et al., 1998), scaled downward by a factor of ten ($f=0.1$), assuming that the laboratory diabase was significantly drier, and therefore stronger, than typical lower crust. The scaled rheology corresponds closely to that of intermediate composition granulite. The upper-mid continental crust has a wet quartzite rheology (Gleason and Tullis, 1995), scaled upward by a factor of five to account for strength differences between the laboratory samples and in-situ crust (Beaumont et al., 2006).

All materials have a density that varies with temperature:

$$\rho(T) = \rho_0[1-\alpha(T-T_0)] \quad (8)$$

Table 1a
Mechanical and thermal parameters for the reference model (Model 1)

Continental plate				Oceanic plate		Sublithospheric mantle	Weak seed
Parameter	Upper/mid crust	Lower crust	Mantle lithosphere	Crust	Mantle lithosphere		
Plastic rheology							
C_0 (MPa)	2	0	0	0	0	0	2
ϕ_{eff}[a]	15° to 2°	15° to 2°	15° to 2°	15° to 2°	15° to 2°	15° to 2°	5°
Viscous rheology							
f	5	0.1	1, 10[b]	0.1	10	1	1
A (Pa^{-n} s^{-1})	1.10×10^{-28}	5.05×10^{-28}	3.91×10^{-15}	5.05×10^{-28}	3.91×10^{-15}	3.91×10^{-15}	1.10×10^{-28}
B^* (Pa^{-n} s^{-1})[c]	2.92×10^{6}	1.91×10^{5}	1.92×10^{4}	1.91×10^{5}	1.92×10^{4}	1.92×10^{4}	2.92×10^{6}
n	4.0	4.7	3.0	4.7	3.0	3.0	4.0
Q (kJ mol^{-1})	223	485	430	485	430	430	223
V^* (cm^3 mol^{-1})	0	0	10	0	10	10	0
Density parameters							
ρ_0 (kg m^{-3})	2800	2950 (3100)[d]	3250	2900 (3300)[d]	3250	3250	3250
T_0 (°C)	200	500 (500)[d]	1344	0 (500)[d]	1344	1344	1344
α (K^{-1})	3.0×10^{-5}	3.0×10^{-5}	3.0×10^{-5}	3.0×10^{-5}	3.0×10^{-5}	3.0×10^{-5}	3.0×10^{-5}
Thermal parameters							
k (W m^{-1})[e]	2.25	2.25	2.25	2.25	2.25	2.25	2.25
A (μW m^{-3})	1.15	0.55	0	0	0	0.0	0.0
c_p (J kg^{-1})	750	750	1250	750	1250	1250	1250

[a] Strain weakening is included with a linear decrease in the effective angle of friction over an accumulated strain, $(I'_2)^{1/2}$ 0.5 to 1.5.
[b] The first value is the backarc block adjacent to the subduction zone; the second value is the stable continent further landward.
[c] $B^*=(2^{(1-n)/n}3^{-(n+1)/2n})A^{-1/n}$. The term in brackets converts the pre-exponential viscosity parameter from uniaxial laboratory experiments (A) to the plane strain conditions of the numerical models. In addition, there is a factor of 2 from the second invariant of the strain rate tensor in Eq. (6) and a factor of 2 from the relationship between effective viscosity and the stress–strain rate ratio.
[d] Values in brackets are for material in the eclogite stability field (Hacker, 1996). The small increase in density for continental lower crust is appropriate for an intermediate composition.
[e] Thermal conductivity for low temperatures (less than 1344°C); at higher temperatures, thermal conductivity increases linearly from 2.25 W m^{-1} K^{-1} at 1344 °C to 52.0 W m^{-1} K^{-1} at 1376 °C.

where ρ_0 is the reference density at temperature T_0 and the thermal expansion coefficient, α, is 3×10^{-5} K^{-1} (Table 1a). In the first set of models, the mantle lithosphere and sublithospheric mantle have identical reference densities that are comparable to primitive mantle (Poudjom et al., 2001). The oceanic crust and lower continental crust undergo a phase change to higher density material when they reach pressures and temperatures within the eclogite stability field (Hacker, 1996) (Table 1a). The phase change affects only density; thermal and mechanical properties are not altered.

Table 1a lists the material thermal parameters. All materials have a thermal conductivity of 2.25 W m^{-1} K^{-1} below 1344 °C (the base of the continental lithosphere at model initiation). Thermal conductivity linearly increases to 52 W m^{-1} K^{-1} at 1376 °C (~200 km depth), corresponding to scaling the thermal conductivity by the Nusselt number of upper mantle convection. The enhanced conductivity maintains a nearly constant heat flux to the lithosphere base and an adiabatic temperature gradient in the sublithospheric mantle (e.g. Pysklywec and Beaumont, 2004). Model tests show that the enhanced thermal conductivity at depth does not strongly influence the development of instabilities. Such instabilities develop and grow near the base of the lithosphere and therefore have long thermal diffusive time constants determined by the 2.25 W m^{-1} K^{-1} thermal conductivity.

2.3. Boundary conditions and initial thermal structure

The coupled thermal–mechanical evolution is solved using Eqs. (1), (2) and (5), with the material properties described above and the following boundary conditions (Fig. 2). Oceanic lithosphere enters through the seaward model boundary at a constant velocity (5 cm/yr in the reference model). The continental lithosphere is pinned at the landward boundary. The top surface of the models is free, and a no-slip condition is used for the basal and side boundaries of the sublithospheric mantle. The side boundaries of the sublithospheric mantle are open, with a small uniform outflux to maintain constant average basal pressure and consequently maintain the total mass in the system. No material is allowed to pass through the basal boundary. The current models do not include interaction between the subducting plate and 660 km phase transition. Instead, subducted material is "absorbed" into the sublithospheric mantle at 550 km depth by changing its mechanical properties to those of sublithospheric mantle and applying a high thermal conductivity (52 W m^{-1} K^{-1}) to reduce its thermal anomaly. This allows models to be run to large convergence with little effect of the basal boundary on slab trajectory; the assumption is that the slab passively enters the lower mantle and does not exert any force on the part that remains in the upper mantle. Slab dynamics at the base of the upper mantle will be the subject of future studies.

The model top boundary has a temperature of 0 °C and the basal boundary temperature is 1560 °C, similar to the inferred temperature at 660 km depth (Thompson, 1992). The incoming oceanic lithosphere has a thickness of 90 km and a prescribed thermal structure consistent with an oceanic plate age greater than 70 Ma (Stein and Stein, 1992). The remaining side boundaries have a no heat flux boundary condition. The initial two-dimensional thermal structure is calculated using these boundary conditions and the material thermal parameters. For the continental plate, the initial thermal structure and lithosphere thickness is similar to that of Phanerozoic continental regions (Chapman and Pollack, 1977; Poudjom et al., 2001), with a Moho temperature (36 km depth) of 568 °C and lithosphere thickness of 120 km (Fig. 2). Surface heat flow is 55 mW/m^2, with 20.8 mW/m^2 vertical heat flux through the sublithospheric mantle.

Subduction is initiated with an inclined weak zone at the boundary between oceanic and continental lithosphere (Fig. 2). After subduction begins, the weak zone material is carried to depth with the subducting plate and does not affect subsequent margin behavior. Models are run to 200 km of plate convergence (4 Ma model time) to fully initiate subduction. The numerical experiments (Table 1b) are carried out starting from this point, assuming that the processes of interest occur on timescales longer than subduction initiation. In all models, we have

Table 1b
List of numerical experiments

Model	Rheology[a]	Density[a]	Subduction rate	Notes
1	Wet Olivine×1	3250	5 cm/yr	
2	Wet Olivine×2	3250	5 cm/yr	
3	Wet Olivine/2	3250	5 cm/yr	
4	Wet Olivine/5	3250	5 cm/yr	
5	Wet Olivine/2	3250	5 cm/yr	No strong continental interior
6	Wet Olivine×1	3230	5 cm/yr	
7	Wet Olivine/2	3230	5 cm/yr	
8	Wet Olivine×1	3270	5 cm/yr	
9	Wet Olivine/2	3270	5 cm/yr	
10	Wet Olivine×1	3250	2 cm/yr	
11	Wet Olivine×1	3250	10 cm/yr	
12	Wet Olivine×1	3250	5 cm/yr	Initial continental Moho: 736 °C
13	Wet Olivine×1	3250	5 cm/yr	Initial continental Moho: 856 °C

[a] Backarc continental mantle lithosphere.

verified that the backarc lithosphere is stable on timescales of 250 Ma in the absence of subduction.

3. Model results

3.1. Reference model

In the reference model (Model 1), the subduction velocity is 5 cm/yr, and the backarc mantle lithosphere and sublithospheric mantle have identical rheologies and compositional densities. Fig. 3 shows the evolution of this model. As the oceanic plate descends, flow is induced in the sublithospheric mantle owing primarily to mechanical traction from the subducting lithosphere. The flow cell consists of downgoing flow immediately above the subducting plate and return flow toward the mantle wedge corner (corner flow). With the temperature-dependent rheology, flow becomes focused upward into the corner, resulting in the mechanical removal of lithosphere, as observed in previous studies (e.g. Furukawa, 1993; Rowland and Davies, 1999; Arcay et al., 2005, 2006).

Further into the backarc, sub-horizontal flow in the sublithospheric mantle shears the lowermost backarc mantle lithosphere, as indicated by the deflection of the initially vertical Lagrangian mesh lines (Fig. 3b). Small perturbations are produced in the thermal and mechanical structure of the lowermost lithosphere, likely caused by heterogeneities in the flow field (Fig. 3c). With progressive shearing, the density perturbations grow in amplitude and become gravitationally unstable. Destabilization occurs as a single downwelling which rapidly grows in amplitude (Fig. 3d–f). As it grows, it is entrained by mantle flow and carried toward the wedge corner. Through the combination of negative buoyancy and entrainment, a thin (~20 km) layer of backarc mantle lithosphere is removed (Fig. 3g).

The thinning process is further illustrated in Fig. 4 which shows the evolution of the average depth of the 1200 °C isotherm in the backarc (x=1000–1450 km). This isotherm is not strongly disturbed by the development of instabilities. Removal of lithosphere occurs within ~8 Ma of the onset of instability. The rapid removal is a consequence of the non-Newtonian lithosphere rheology, which allows for a super-exponential instability growth rate (Houseman and Molnar, 1997). After the initial removal event, the remaining mantle lithosphere, which is not in thermal equilibrium, begins to heat conductively from below. The temperature increase weakens the lowermost lithosphere, resulting in a second, more muted, phase of instability at ~50 Ma (Fig. 4).

3.2. Variations in backarc mantle lithosphere rheology

We first examine the sensitivity of the models to variations in backarc mantle lithosphere strength by using the factor (f) to scale the viscosity relative to the reference wet olivine (Eq. (6)). In Model 2, the backarc mantle lithosphere viscosity is scaled upward by a factor of

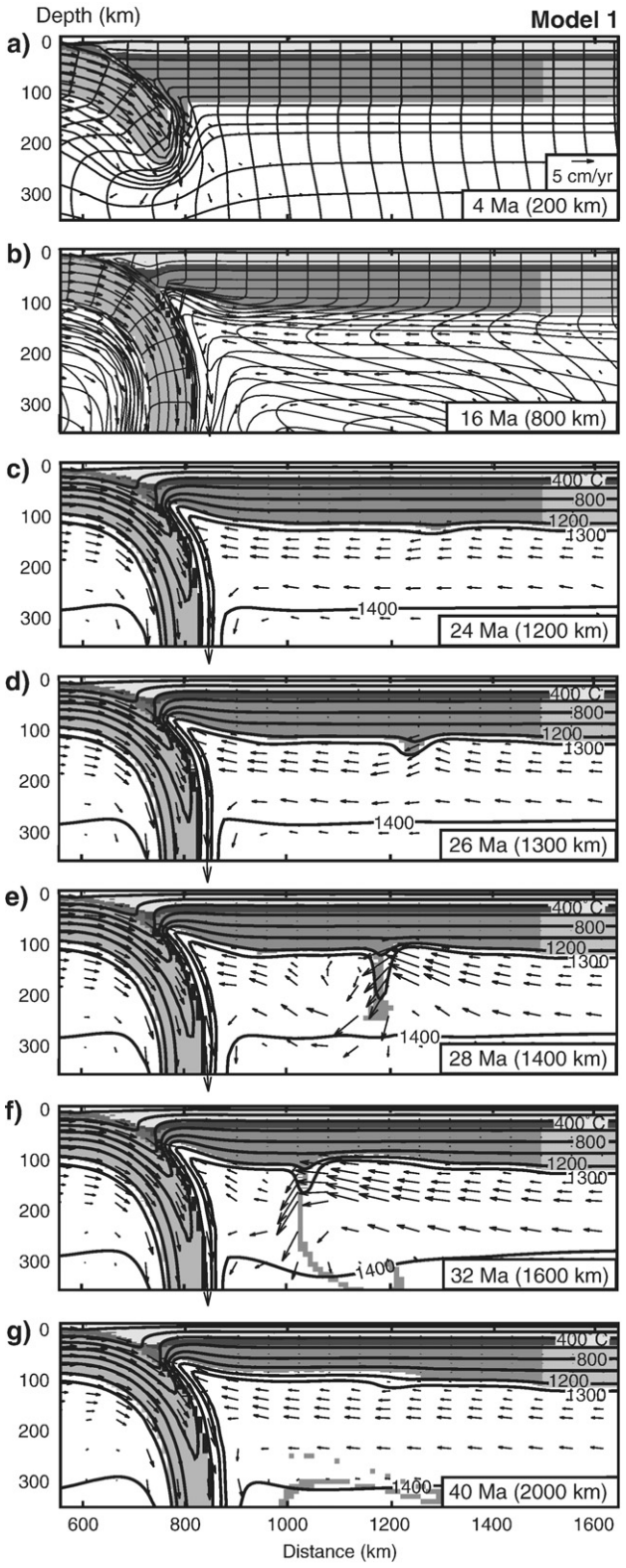

Fig. 3. Evolution of Model 1 (reference model) showing the development of gravitational instability and removal of the lowermost backarc lithosphere. The Lagrangian mesh (originally composed of undeformed rectangular cells) is shown in (a) and (b), plotted at 1/6 the actual resolution. The elapsed time since subduction initiation is shown in the bottom right corner of each panel with the amount of convergence in brackets. There is no vertical exaggeration. The higher velocity vector density in the upper 180 km reflects the smaller vertical element size here.

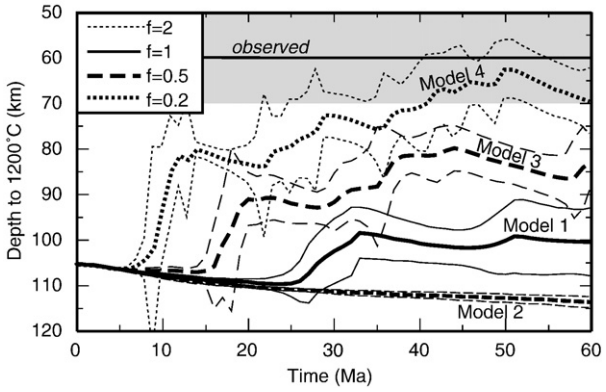

Fig. 4. Effect of mantle lithosphere rheology on the evolution of the average depth of the 1200 °C isotherm for the backarc. Thin lines show the $1-\sigma$ variation in depth. All models use a wet olivine dislocation creep rheology (Karato and Wu, 1993) and the relative strength is varied with the viscosity scaling factor, f (Eq. (6)).

two (wet olivine×2). Fig. 5 shows the model at 60 Ma after subduction initiation. With the higher viscosity, ablation of the wedge corner by mantle flow is reduced relative to the reference model. Arcay et al. (2005, 2006) observed a similar relationship between lithosphere rheology and amount of ablation. The backarc mantle lithosphere does not undergo gravitational instability over the 60 Ma model time, as reflected by the smooth evolution of the 1200 °C isotherm depth (Fig. 4). The slight increase in depth with time is due to secular cooling of the model (see Section 5).

In Model 3, the backarc mantle lithosphere has a viscosity half that of the reference model (f=0.5 or wet olivine/2). The weaker rheology allows a greater amount of ablation of the wedge corner (Fig. 6a). In the backarc, mantle flow shears the lowermost lithosphere, producing perturbations which develop into rapidly-growing, gravitational downwellings (Fig. 6b). Two distinct downwellings develop and are entrained by the underlying mantle flow (Fig. 6c–i). Within 6 Ma, the downwellings detach, removing nearly 35 km of mantle lithosphere. The remaining lithosphere begins to heat conductively, leading to a second phase of thinning (Fig. 6j). The two phases are clearly shown in the evolution of the 1200 °C isotherm depth (Fig. 4). The initial thinning event occurs at ~15 Ma and is characterized by a rapid decrease in the 1200 °C isotherm depth. This is followed by the second, slower phase of thinning at ~29 Ma.

If the backarc mantle lithosphere is even weaker, wet olivine/5 (f=0.2) (Model 4), the lithosphere is much more unstable, with the onset of instability at ~8 Ma (Fig. 4). By 45 Ma, the 1200 °C isotherm in the backarc is at a depth of ~65 km.

As shown in Fig. 6j, thinning occurs across the full width of the backarc lithosphere block. The landward extent is limited by the continental interior mantle lithosphere, which has a rheology of wet olivine×10 and is too strong to destabilize. We have examined a model where there is no strong interior; all continental mantle lithosphere has a wet olivine/2 rheology (Model 5). Lithosphere thinning occurs on the same timescales as Model 3, with comparable amounts of lithosphere removal, but thinning affects the entire width of continental lithosphere.

3.3. Variations in continental mantle lithosphere density

The observed lithosphere thinning occurs primarily through gravitationally-driven downwellings, and therefore depends on lithosphere density structure. In the above models, the mantle lithosphere and sublithospheric mantle have the same reference density and thus, instability is driven by the negative buoyancy associated with cooler lithosphere temperatures. We now consider different compositional densities.

During lithosphere formation and evolution, extensive melting may produce chemical depletion, as iron and other heavy elements are extracted (e.g. Jordan, 1978). As a result, the residual mantle lithosphere may be less dense than undifferentiated mantle. We have conducted experiments in which the reference density of the continental mantle lithosphere is 20 kg/m^3 less than that of the sublithospheric mantle, similar to the density difference between primitive mantle and Phanerozoic continental mantle (Poudjom et al., 2001). Model 6 has a backarc mantle lithosphere rheology of wet olivine×1. Induced mantle flow shears the backarc lithosphere, but the compositional buoyancy of the lithosphere is sufficient to prohibit gravitational instability (Fig. 7a). If the backarc mantle lithosphere viscosity is decreased by a factor of two (Model 7), mantle flow shears a thicker layer of the lithosphere and some thinning occurs through entrainment, but again compositional buoyancy prevents instability (Fig. 7b).

An alternate model for continental lithosphere growth is the stacking of subducted oceanic plates (Bostock, 1998), such that eclogitized oceanic crust may be embedded in the lithosphere, increasing its intrinsic density. The next models examine a continental mantle lithosphere with a reference density of 3270 kg/m^3, 20 kg/m^3 greater than the sublithospheric mantle. With the increased density, the instability of the backarc mantle lithosphere is enhanced for lithosphere rheologies of wet olivine×1 (Model 8) and wet olivine/2 (Model 9). Relative to models with a 3250 kg/m^3 lithosphere reference density, the onset of gravitational instability occurs earlier and the amount of thinning is larger (Fig. 7a,b).

3.4. Variations in subduction rate

A key factor controlling lithosphere thinning is the subduction-related flow field in the sublithospheric mantle. The above models have a moderate subduction rate of 5 cm/yr. The next models

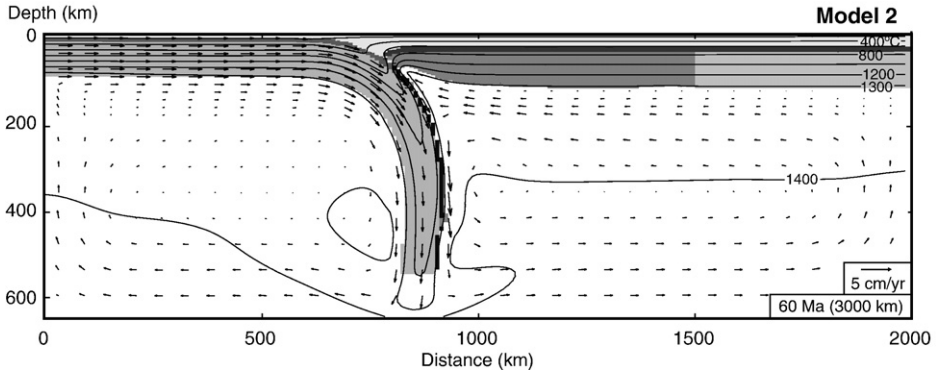

Fig. 5. Model 2 at 60 Ma after subduction initiation. The entire model domain is shown. With a wet olivine×2 rheology, the backarc mantle lithosphere does not undergo gravitational destabilization.

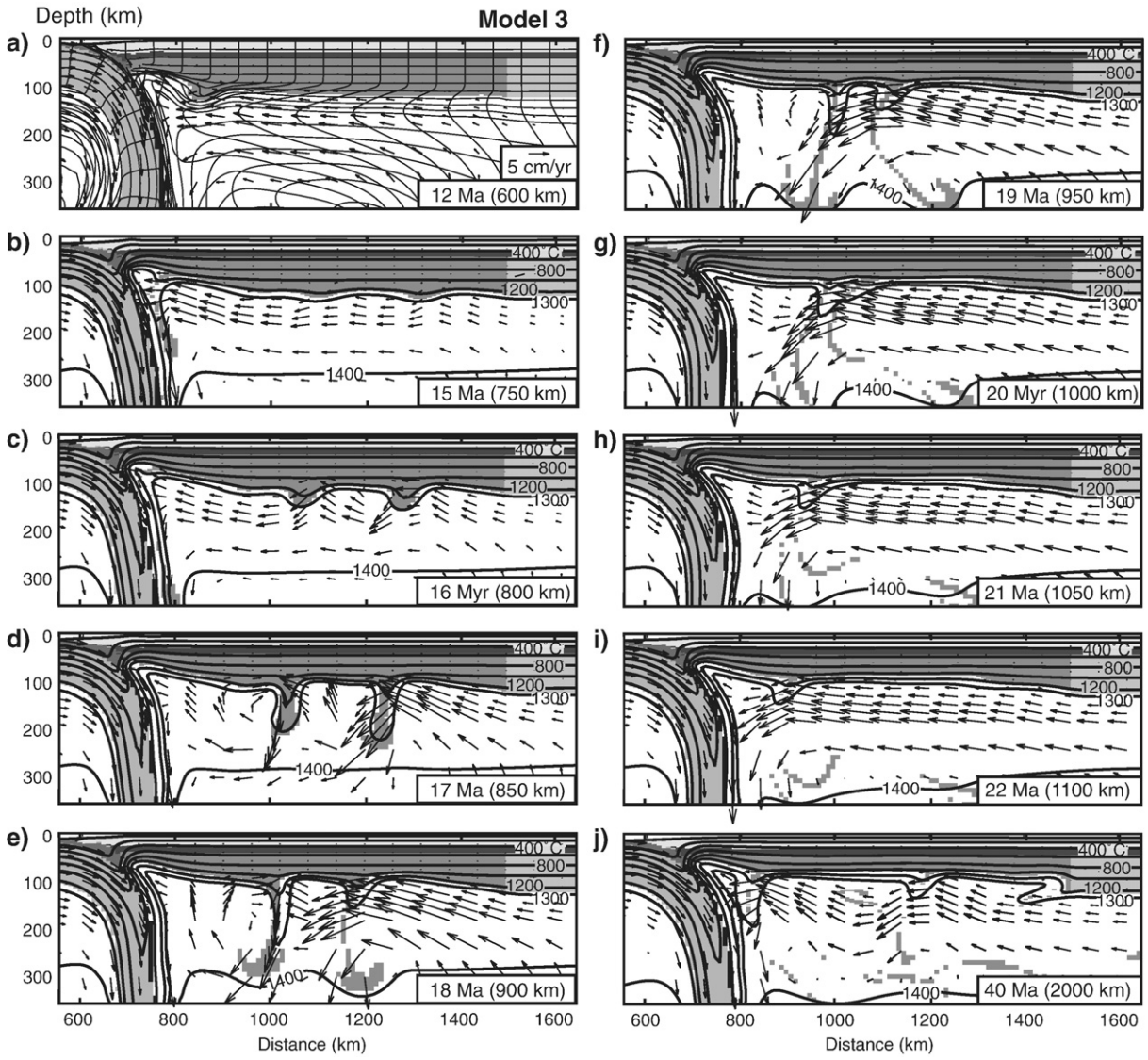

Fig. 6. Evolution of Model 3, where the backarc mantle lithosphere has a rheology of wet olivine/2. With the weak rheology, gravitational instabilities initiate earlier than in the reference model and grow at a faster rate, removing more lithosphere. The thinned lithosphere then heats conductively and undergoes a second phase of thinning, resulting in thinning over the entire width of the predefined backarc region (plot j).

investigate variations in subduction rate, with all other parameters identical to the reference model. With a 2 cm/yr subduction rate (Model 10), the onset of gravitational instability is delayed by ~6 Ma and the initial phase of thinning takes slightly longer, relative to the reference model (Fig. 7c). In contrast, for a higher subduction rate of 10 cm/yr (Model 11), gravitational instability develops ~4 Ma sooner and the downwelling is removed more quickly (Fig. 7c). Overall, the amount of lithosphere removed in the initial thinning event is similar for all models.

3.5. Variations in initial thermal structure

The final models investigate variations in continental lithosphere temperatures. The above models have a thermal structure similar to average Phanerozoic continental lithosphere (Poudjom et al., 2001). However, some continental regions may be hotter, due to enhanced crustal radioactive heat production or high transient temperatures associated with an episode of lithosphere thickening and associated radioactive self-heating. We have constructed models with a hotter lithosphere by increasing the radioactive heat production in the crust, while decreasing the mantle heat flow to maintain an initial lithosphere thickness of 120 km. All other parameters are the same as the reference model.

In Model 12, heat production in the upper and lower continental crust is twice that of the reference model (2.3 and 1.1 $\mu W/m^3$, respectively) and the mantle heat flow is 16.6 mW/m^2. This yields an initial continental Moho temperature of 736 °C and surface heat flow of 85 mW/m^2. With the higher temperatures, the lithosphere has a lower viscosity than the reference model, making it more unstable. The first phase of gravitational instability begins at ~19 Ma after subduction initiation, approximately 7 Ma earlier than the reference model (Fig. 8a). By 40 Ma, the backarc lithosphere is appreciably thinner (Fig. 8b) and at 60 Ma, the 1200 °C isotherm is ~25 km shallower than the reference model (Fig. 8a).

Model 13 has an even hotter thermal structure, with an initial continental Moho temperature of 856 °C and 94 mW/m^2 surface heat flow. This model has radioactive heat production of 2.25 $\mu W/m^3$ for the entire continental crust and mantle heat flow of 13 mW/m^2, similar to the inferred mantle heat flow below cratons (Jaupart and Mareschal, 1999). With the elevated temperatures, the lithosphere is highly unstable. Gravitational instability initiates at ~12 Ma, followed by a second phase of thinning at ~25 Ma (Fig. 8a). By 40 Ma, nearly all

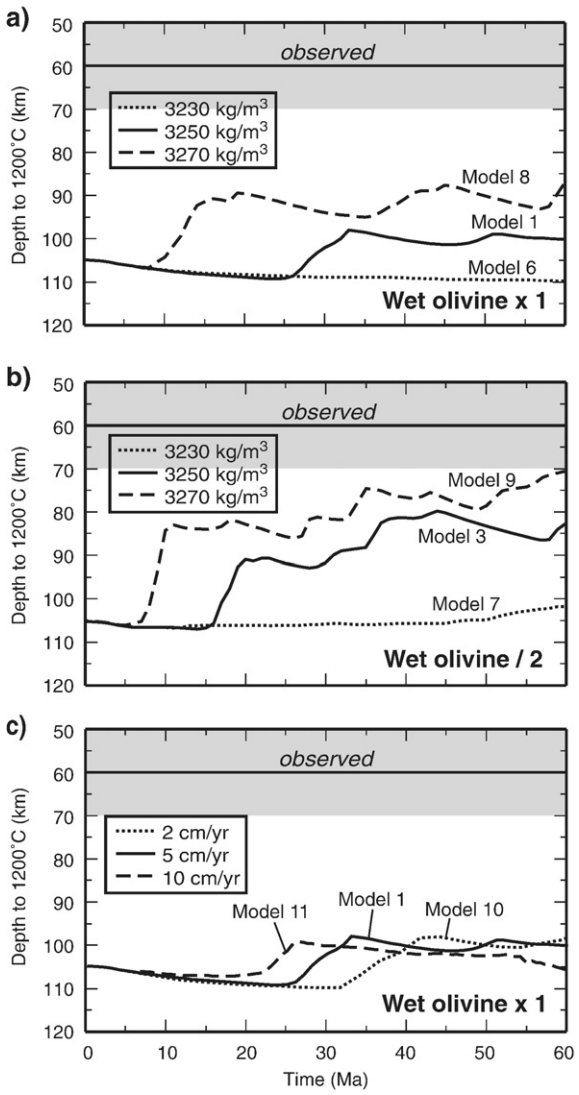

Fig. 7. Evolution of the average depth of the 1200 °C isotherm for the backarc for a) variations in continental mantle lithosphere density with a wet olivine (×1) rheology, b) variations in density with a wet olivine/2 rheology, and c) variations in subduction velocity with a wet olivine (×1) rheology.

the backarc mantle lithosphere has been removed (Fig. 8c) and the 1200 °C isotherm is at 55–60 km depth (Fig. 8a). Our results are compatible with the models of Morency and Doin (2004) which show the near-complete removal of mantle lithosphere for Moho temperatures greater than 800 °C.

4. Scaling analysis for shear-induced gravitational instability

4.1. Reference model

Two key factors appear to contribute to the destabilization and removal of backarc lithosphere in models that are otherwise stable on a 250 Ma timescale. Firstly, heterogeneities in the subduction-induced mantle flow regime (e.g., non-horizontal flow related to ablation of the mantle wedge corner) cause small amplitude perturbations to the lower backarc lithosphere. Secondly, the associated high shear strain rates result in strain rate softening and a decrease of the effective viscosity of the lower lithosphere, owing to its power-law rheology. The viscosity decrease enables the small density perturbations to become gravitationally unstable, resulting in lithosphere thinning.

To quantify the effect of strain rate softening by basal shearing on lithosphere instability, we have developed a buoyancy scaling analysis. The gravitational stability of mantle lithosphere depends on the relative magnitude of its negative buoyancy, which drives instability, and its viscosity structure, which acts to stabilize the lithosphere. Conrad and Molnar (1999) showed that the gravitational stability of a lithosphere layer of thickness h can be represented by a non- dimensional number, Ra_1:

$$Ra_1 = \frac{\rho_m g \alpha \Delta T h^3 F_1}{2\kappa\eta_m} \tag{9}$$

where ΔT is the temperature difference across the layer, g is the gravitational acceleration, α is the thermal expansion coefficient, κ is the thermal diffusivity, and ρ_m and η_m are the density and viscosity, respectively, at the base of the lithosphere. This number is similar to the standard Rayleigh number with the additional factor, F_1, which is the "available buoyancy" of the layer. F_1 is calculated by integrating the ratio of the negative buoyancy of the layer by the inverse of its viscosity coefficient (Conrad and Molnar, 1999). This weights the relative contributions of negative buoyancy and viscosity for boundary layers with vertical temperature gradients; areas of low temperature will have a large negative buoyancy but will also have a high viscosity, and thus may not be able to drive instability. Numerical experiments show that a layer will be unstable if Ra_1 is greater than 100 (Conrad and Molnar, 1999; Conrad, 2000).

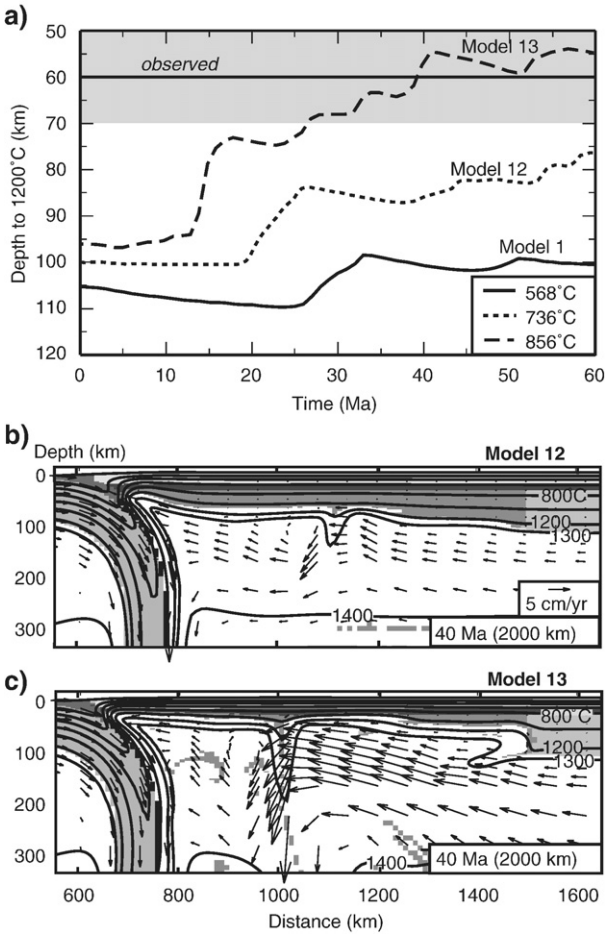

Fig. 8. a) Effect of initial continental thermal structure on the evolution of the average depth of the 1200 °C isotherm for the backarc. The initial thermal structure is given by the continental Moho temperature. b) Model 12 (736 °C Moho) and c) Model 13 (856 °C Moho) at 40 Ma.

In our models, the lithosphere density profile is determined by the thermal structure, while the effective viscosity profile is given by both temperature and the background strain rate associated with basal shearing. The strain rate profile for the reference model shows an upward exponential decrease in strain rate, with an e-folding length scale (D_b) of ~4.5 km (Fig. 9a). D_b is relatively insensitive to variations in shearing rate, viscosity scaling factor and lithosphere compositional density, but increases if the lithosphere temperature gradient decreases. With the strain rate variation, the lower lithosphere will experience greater amounts of strain rate weakening. To account for this, we have modified the viscosity coefficient in the available buoyancy calculations (Conrad and Molnar, 1999) to include the upward decrease in strain rate.

Fig. 9b shows the calculated Ra_1 as a function of layer thickness (measured from the lithosphere base) for different basal shearing velocities. The associated basal strain rate was determined assuming simple shear throughout the lithosphere. At low velocities (<0.02 cm/yr), the analysis predicts that the entire mantle lithosphere will be stable, with Ra_1<100 for all thicknesses. This agrees with the model results which show that the lithosphere is stable in the absence of subduction. In the reference model (Model 1), flow velocities at the backarc lithosphere base are ~1.2 cm/yr. For this velocity, the calculations indicate that the critical Ra_1 of 100 is reached for a layer thickness of ~21 km (h_{crit}). Initial growth rates will be exponential but grow to become super-exponential when the strain rate associated with the instability exceeds that induced by basal shear (Houseman and Molnar, 1997; Molnar et al., 1998).

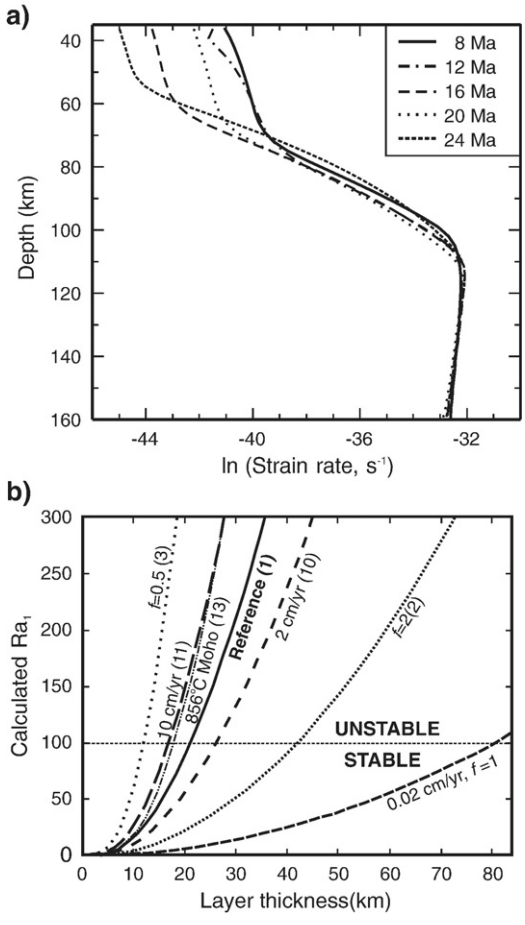

Fig. 9. a) Average backarc strain rate profiles (x=1000 to 1450 km) for Model 1 prior to destabilization. The natural log of the strain rate is plotted. The lithosphere strain rate decreases exponentially upward. b) Predicted stability (Ra_1) as a function of layer thickness (measured from the base of the lithosphere) for variations in subduction rate, viscosity scaling factor (f), and Moho temperature. The model number corresponding to each curve is given in brackets. The critical layer thickness (h_{crit}) occurs at Ra_1=100, and indicates the minimum lithosphere thickness that may be removed by instability.

The thickness h_{crit} is an estimate of the minimum amount of lithosphere that may be removed by the instability. Larger thicknesses are also potentially unstable (Ra_1>100 in Fig. 9b), but rapid growth of a larger instability also depends on the flow perturbation; i.e. an 'effective perturbation' will be required that has an appropriate wavelength and perturbs a greater thickness of lithosphere (Conrad and Molnar, 1999). Lacking details of the perturbation, we can only estimate h_{crit}. However, given that flow-driven shearing decreases exponentially upward from the base of the lithosphere (Fig. 9a), the amount of lithosphere that will be effectively perturbed may not be much larger than h_{crit}. This is supported by the reference model, h_{crit}=21 km, which is comparable with the numerical model results (Fig. 3). However, in cases where the lithosphere is weaker, h_{crit} underestimates the thickness of the layer that is removed. There is clearly a tradeoff between increasing h_{crit} values with decreasing lithospheric instability and the ability to effectively perturb such thick layers.

4.2. Effect of subduction velocity

Variations in subduction rate affect the basal shearing velocity and hence the magnitude of strain rate weakening of the backarc lithosphere. For example, at 20 Ma, higher velocities (Model 11, 10 cm/yr subduction rate) reduce the lowermost lithosphere effective viscosity by a factor of 1.9, whereas lower velocities (Model 10, 2 cm/yr subduction rate) increase the effective viscosity by 1.5. The predicted stability curves for the corresponding basal shearing velocities of 0.6 cm/yr (Model 10) and 2.3 cm/yr (Model 11) indicate a minor decrease in h_{crit} at higher velocities, suggesting a slightly more unstable lithosphere (Fig. 9b). In addition, the perturbation magnitude likely increases as the flow velocities increase, further enhancing the instability. The result is that a higher subduction rate leads to an earlier onset of destabilization, larger initial growth rate, and shorter instability removal times for higher velocities, in agreement with model results (Fig. 7c).

4.3. Effect of viscosity scaling factor, temperature and compositional density

The buoyancy scaling analysis also provides insight into the effects of other model parameters. In the models, the onset of instability was found to be strongly dependent on the viscosity scaling factor (f). At larger f, the increased lithosphere stability appears to result from: 1) reduced perturbation of the lithosphere due to its increased strength, and 2) an increase in Ra_1 associated with both an increase in the background lithosphere viscosity by factor f and a decrease in basal shearing velocity, as it is more difficult for the stronger lithosphere to be sheared by mantle flow.

For Model 2 (f=2, 0.4 cm/yr shearing velocity), the stability analysis predicts h_{crit}=42 km (Fig. 9b). However, no instability was observed (Fig. 5). This is likely because the minimum thickness that will be unstable is large (42 km); probably larger than the thickness of the layer actually perturbed by the shear flow. That is, the 'effective perturbation' is limited to only a thin layer at the base of the lithosphere, owing to the strong rheology, low basal shearing velocity, and localization of strain rate weakening in the lowermost lithosphere. In contrast, weaker lithospheres have a lower h_{crit} (e.g., Model 3 in Fig. 9b, f=0.5, 3.5 cm/yr shearing velocity, h_{crit}=16 km), and this thinner layer will be more easily perturbed by the shear flow. In this case, the actual amount removed was larger than h_{crit} (Fig. 4), indicating that under some circumstances more than the minimum thickness can be effectively perturbed.

Variations in lithosphere thermal structure have a similar effect as scaling the viscosity, as temperature exerts a primary control on

viscosity. Fig. 9b shows the stability curve for Model 13, which has a Moho temperature of 856 °C. The hot, weak lithosphere is more easily sheared by mantle flow, with basal shearing velocities of 2.4 cm/yr. Even though the lithosphere density gradient is reduced, the higher temperatures, the temperature-related decrease in effective viscosity, the reduced upward viscosity gradient associated with shearing (D_b=7.0 km) and the increased shearing velocity produce a low h_{crit} of 17 km. Furthermore, it is expected that a hot lithosphere will be more prone to perturbation by flow. These factors result in an increase in lithosphere instability, higher instability growth rates, and increased thickness of lithosphere removed relative to cooler models.

Finally, the models show that the compositional density contrast between the lithosphere and sublithospheric mantle also affects lithosphere stability. Even moderate compositional buoyancy of the mantle lithosphere will offset the negative buoyancy owing to lower temperatures, and thus the lithosphere will be gravitationally stable, although some thinning may occur through shear flow entrainment of the strain-rate-weakened lower lithosphere (Fig. 7). Conversely, instability can be enhanced for a lithosphere that has a larger intrinsic density than the sublithospheric mantle.

5. Discussion

5.1. Lithosphere instability in backarcs

From comparison of the numerical model results with the scaling analysis, we interpret the observed backarc lithosphere thinning to be a consequence of shearing of the lithosphere by subduction-induced mantle flow. Flow creates perturbations in the density field which grow into gravitational instabilities because shear flow also reduces the effective viscosity through strain rate softening. In contrast, modeling studies of small-scale convection below moving oceanic plates find that shearing between the lithosphere and sublithospheric mantle either has little effect on instability (Dumoulin et al., 2005) or may hinder the development of instabilities (Huang et al., 2003; van Hunen et al., 2003). The likely explanation for the difference in behaviour is that these studies use a Newtonian lithosphere rheology, and thus, the lithosphere effective viscosity does not decrease with shearing.

In addition, the two-dimensional models described here cannot address components of the flow that are three dimensional, for example the effect of toroidal flow caused by retreat of the subducting plate (e.g., Kincaid and Griffiths, 2003; Stegman et al., 2006; Funiciello et al., 2006). Such components may also contribute to enhanced lower lithosphere shearing and promote gravitational instabilities.

In our models, once the lithosphere becomes unstable, thinning occurs in two phases: an initial phase of gravitational instability where significant thinning occurs in 5–10 Ma, and a second, slower phase of gravitational thinning of the remaining lithosphere as it is weakened by both conductive heating from below and shearing by mantle flow. In this phase, the amount of lithosphere removal decreases with time, and by 60 Ma, the lithosphere is likely close to its stable steady-state thickness. Mantle flow associated with ongoing subduction may provide a mechanism to maintain the thinned lithosphere over longer timescales (Hyndman et al., 2005).

We note that the amount of thinning during the second phase may be underestimated in the models. Ongoing subduction of the cool oceanic plate results in secular cooling, as reflected by the gradual increase in the 1200 °C isotherm depth in Model 2 (Fig. 4). The slow cooling will strengthen the lithosphere, reducing its susceptibility to thinning. Secular cooling becomes significant at times greater than 30–40 Ma. In the models, the majority of thinning occurs within 30 Ma of subduction initiation and thus secular cooling should not alter the main conclusions of this study.

An important question is whether thinning by shearing and gravitational instability can result in backarc lithosphere with the observed thickness and thermal structure of many continental backarcs (i.e. 1200 °C at ~60 km depth (Currie and Hyndman, 2006)). One way to produce this thermal structure is with a backarc mantle lithosphere that has a weak rheology of wet olivine/5 (Fig. 4). A comparison between the olivine flow law used in the models (Karato and Wu, 1993) and flow laws that explicitly include a term for water content (e.g., Hirth and Kohlstedt, 1996) indicates that the wet olivine/5 rheology is a factor of ~2 weaker than water-saturated mantle at 100–120 km depth. A factor of 2 is probably much smaller than the uncertainties associated with extrapolating laboratory data to natural conditions, therefore weak lithosphere associated with a wet olivine rheology remains a possible reason for the thinning. Thinning can also be enhanced if the lithosphere has a compositional density larger than that of the sublithospheric mantle. However, even for a compositional density increase of 20 kg/m^3, lithosphere weaker than wet olivine/2 would be required (Fig. 8b). Significant thinning also occurs if the average mantle lithosphere temperature is ~150 °C hotter than typical Phanerozoic continental lithosphere (Fig. 9). This thermal structure, with an 856 °C Moho, is likely an end-member for most continental regions, but may result from lithospheric shortening and crustal thickening in Cordilleran orogenesis, of which the Central Andes is a type example. Alternatively, a combination of weak lithosphere rheology and a thermal structure somewhat warmer than average Phanerozoic lithosphere may be sufficient to produce the observed backarc lithosphere thickness.

5.2. Application to Western North America

Shear-induced instability may be limited to continental lithosphere that is both rheologically weak and has a compositional density similar to, or greater than, sublithospheric mantle. This requirement can be achieved in lithosphere that contains a small amount of water and other volatiles, and that is fertile. By implication, only lithosphere that has not undergone extensive melting during its formation and evolution may be susceptible to destabilization in a backarc setting. Extensive melting and melt extraction result in chemical depletion (Jordan, 1978) and devolatization (Pollack, 1986), such that the residual lithosphere is compositionally buoyant, has a high viscosity, and is therefore gravitationally stable (Doin et al., 1997). Support for a compositional control on stability comes from xenolith data that show that the tectonically-active southern Basin and Range is underlain by a thin, fertile lithosphere, whereas the undeformed Colorado plateau has a thicker, more depleted lithosphere (Lee et al., 2001).

In western Canada, thin lithosphere is found beneath the present-day Cascadia backarc and the Canadian Cordillera further north, which was a backarc region until 40–45 Ma (Engebretson et al., 1985) (Fig. 1b). The thin lithosphere coincides with the extent of terranes that were accreted to the western margin of the North American craton (Gabrielse and Yorath, 1992; Hyndman and Lewis, 1999; Monger and Price, 2002). Geochemical analyses of lherzolite mantle xenoliths from Late Tertiary to Recent volcanic fields in the Cascadia backarc (Fig. 1b) indicate a fertile composition, with an Mg number of 0.89–0.90 (Peslier et al., 2000). This is only slightly larger than that of the convecting mantle (Mg#=0.88 (Lee et al., 2001)). To the north, geochemical and isotopic studies of Tertiary to Recent alkaline basaltic lavas, interpreted to originate in the mantle lithosphere, also indicate an enriched and fertile composition (Fig. 1b), in agreement with mantle xenolith geochemistry for this area (Abraham et al., 2001 and references therein).

The eastern limit of thin lithosphere, defined by geophysical studies, coincides with the Rocky Mountain Trench and its northern extension, the Tintina Fault (Fig. 1b). In the Watson Lake region of the Tintina Fault, there is a dramatic change in alkaline basaltic magma geochemistry, from a fertile mantle source west of the fault to depleted mantle on the east (Abraham et al., 2001). These data suggest that the Tintina Fault is a steeply-dipping, lithospheric-scale feature

that juxtaposes lithospheres of different compositions and geophysical properties (Abraham et al., 2001; Zelt et al., 2006). Further east, mantle xenoliths from the shallow (<200 km) lithosphere of the western North American craton have Mg # of 0.92–0.93 (Griffin et al., 2004), indicative of a depleted mantle composition. The refractory, depleted composition of the North American craton mantle lithosphere may make it compositionally buoyant and rheologically strong, and thus resistant to destabilization (e.g. Jordan, 1978; Doin et al., 1997; Poudjom et al., 2001; Lee et al., 2001; Lee et al., 2005). Hence, evidence from the western Canadian Cordillera is consistent with our observation that only wet, fertile lithospheric mantle may be susceptible to thinning by basal shear flow.

6. Conclusions

Numerical models show that shearing of backarc lithosphere by subduction-induced mantle flow can trigger gravitational instability within 30 Ma of subduction initiation. Two factors appear to contribute to destabilization: 1) flow produces small density perturbations in the lower lithosphere, and 2) shearing of the lithosphere decreases its effective viscosity, owing to its power-law rheology. With the decreased viscosity, the gravitationally-driven growth rate of the density perturbations exceeds the rate of shearing, resulting in removal of the lowermost lithosphere. Model results show that instability is enhanced at larger subduction rates, and for lithospheres with a weak intrinsic rheology, high Moho temperatures, and a compositional density equal to, or greater than, the sublithospheric mantle. Through gravitational downwelling, the lowermost backarc lithosphere can be removed within 10 Ma. This is followed by a second phase of gravitational thinning, as the remaining lithosphere is weakened by conductive heating from below and by ongoing shearing.

Lithospheric thinning in this manner may be restricted to mantle lithosphere that has a weak rheology, perhaps due to the presence of water and other volatiles, and that has a fertile composition. Significant thinning of backarc lithosphere (i.e., to produce a temperature of 1200 °C at 60 km depth) may also require lithosphere temperatures somewhat hotter than average Phanerozoic continental regions. For the Canadian Cordillera, the thin lithosphere appears to be confined to terranes accreted to the North American craton and limited geochemical data suggest a fertile mantle lithosphere. The adjacent North American craton has a depleted composition and thus may be compositionally buoyant, rheologically strong and resistant to destabilization. If the proposed mechanism has operated in other backarcs, the area of thin backarc lithosphere should correlate with regions that have a fertile, hydrated continental mantle lithosphere.

Acknowledgements

We thank the two anonymous reviewers for their comments which allowed us to improve the scope and clarity of the manuscript. This research was supported by an NSERC postdoctoral fellowship to Claire Currie, the Canada Research Chair in Geodynamics to Chris Beaumont and an IBM SUR Grant.

References

Abraham, A., Francis, D., Polve, M., 2001. Recent alkaline basalts as probes of the lithospheric mantle roots of the northern Canadian Cordillera. Chem. Geol. 175, 361–386.

Allmendinger, R.W., Jordan, T.E., Kay, S.M., Isacks, B.L., 1997. The evolution of the Altiplano–Puna Plateau of the Central Andes. Annu. Rev. Earth Planet. Sci. 25, 139–174.

Arcay, D., Tric, E., Doin, M.P., 2005. Numerical simulations of subduction zones: effect of slab dehydration on the mantle wedge dynamics. Phys. Earth Planet. Int. 149, 133–153.

Arcay, D., Doin, M.P., Tric, E., Bousquet, R., de Capitani, C., 2006. Overriding plate thinning in subduction zones: localized convection induced by slab dehydration. Geochem. Geophys. Geosys. 7. doi:10.1029/2005GC001061.

Beaumont, C., Nguyen, M., Jamieson, R., Ellis, S., 2006. Crustal flow modes in large hot orogens. In: Law, R.D., Searle, M.P., Godin, L. (Eds.), Crustal Flow, Ductile Extrusion and Exhumation in Continental Collision Zones. Special Publication, vol. 268. Geological Society of London, London, pp. 91–145.

Bird, P., 1979. Continental delamination and the Colorado Plateau. J. Geophys. Res. 84, 7561–7571.

Bostock, M.G., 1998. Mantle stratigraphy and evolution of the Slave province. J. Geophys. Res. 103, 21183–21200.

Cadek, O., Fleitout, L., 2003. Effect of lateral viscosity variations in the top 300 km on the geoid and dynamic topography. Geophys. J. Int. 152, 566–580.

Chapman, D.S., Pollack, H.N., 1977. Regional geotherms and lithospheric thickness. Geology 5, 265–268.

Conrad, C.P., 2000. Convective instability of thickening mantle lithosphere. Geophys. J. Int. 143, 52–60.

Conrad, C.P., Molnar, P., 1999. Convective instability of a boundary layer with temperature- and strain-rate-dependent viscosity in terms of "available buoyancy". Geophys. J. Int. 139, 51–68.

Currie, C.A., Hyndman, R.D., 2006. The thermal structure of subduction zone back arcs,. J. Geophys. Res. 111. doi:10.1029/2005JB004024.

Dixon, J.E., Dixon, T.H., Bell, D.R., Malservisi, R., 2004. Lateral variation in upper mantle viscosity: Role of water. Earth Planet. Sci. Lett. 222, 451–467.

Doin, M.P., Fleitout, L., Christensen, U., 1997. Mantle convection and stability of depleted and undepleted continental lithosphere. J. Geophys. Res. 102, 2771–2787.

Dumoulin, C., Doin, M.P., Arcay, D., Fleitout, L., 2005. Onset of small-scale instabilities at the base of the lithosphere: scaling laws and role of pre-existing lithospheric structures. Geophys. J. Int. 160, 344–356.

Engebretson, D.C., Cox, A., Gordon, R.G., 1985. Relative Motions between Oceanic and Continental Plates in the Pacific Basin, Special Paper 206. Geological Society of America, Denver, CO. (59 pp.).

Fullsack, P., 1995. An arbitrary Lagrangian–Eulerian formation for creeping flows and its application in tectonic models. Geophys. J. Int. 120, 1–23.

Funiciello, F., Moroni, M., Piromallo, C., Faccenna, C., Cenedese, A., Bui, H.A., 2006. Mapping mantle flow during retreating subduction: laboratory models analyzed by feature tracking. J. Geophys. Res. 111. doi:10.1029/2005JB003792.

Furukawa, Y., 1993. Depth of the decoupling plate interface and thermal structure under arcs. J. Geophys. Res. 98, 20005–20013.

Gabrielse, H., Yorath, C.J. (Eds.), 1992. Geology of the Cordilleran Orogen in Canada, Part B. The Geology of North America, vol. G-2. Geological Society of America, Boulder, CO (844 pp.).

Garzione, C.N., Molnar, P., Libarkin, J.C., MacFadden, B.J., 2006. Rapid late Miocene rise of the Bolivian Altiplano: evidence for removal of mantle lithosphere. Earth Planet. Sci. Lett. 241, 543–556.

Gleason, G.C., Tullis, J., 1995. A flow law for dislocation creep of quartz aggregates determined with the molten salt cell. Tectonophysics 247, 1–23.

Griffin, W.L., O'Reilly, S.Y., Doyle, B.J., Pearson, N.J., Coopersmith, H., Kivi, K., Malkovets, V.G., Pokhilenko, N.P., 2004. Lithosphere mapping beneath the North American Plate. Lithos 77, 873–922.

Hacker, B.R., 1996. Eclogite formation and the rheology, buoyancy, seismicity, and H_2O content of oceanic crust. In: Bebout, G.E., Scholl, D.W., Kirby, S.H., Platt, J.P. (Eds.), Subduction top to bottom. Geophysical Monograph, vol. 96, pp. 337–346.

Hirth, G., Kohlstedt, D.L., 1996. Water in the oceanic upper mantle: implications for rheology, melt extraction and the evolution of the lithosphere. Earth Planet. Sci. Lett. 144, 93–108.

Hirth, G., Kohlstedt, D., 2003. Rheology of the upper mantle and mantle wedge: a view from the experimentalists. In: Eiler, J. (Ed.), Inside the subduction factory. Geophysical Monograph, vol. 138. American Geophysical Union, Washington, DC, pp. 83–105.

Houseman, G.A., McKenzie, D.P., Molnar, P., 1981. Convective instability of a thickened boundary layer and its relevance for the thermal evolution of continental convergent belts. J. Geophys. Res. 86, 6115–6132.

Houseman, G.A., Molnar, P., 1997. Gravitational (Rayleigh–Taylor) instability of a layer with non- linear viscosity and convective thinning of continental lithosphere. Geophys. J. Int. 128, 125–150.

Huang, J., Zhong, S., van Hunen, J., 2003. Controls on sublithospheric small-scale convection. J. Geophys. Res. 108. doi:10.1029/2003JB002456.

Huismans, R.S., Beaumont, C., 2003. Symmetric and asymmetric lithospheric extension: relative effects of frictional-plastic and viscous strain softening. J. Geophys. Res. 108. doi:10.1029/2002JB002026.

Hyndman, R.D., Lewis, T.J., 1999. Geophysical consequences of the Cordillera–Craton thermal transition in southwestern Canada: thermal regimes in the continental and oceanic lithosphere. Tectonophysics 306, 397–422.

Hyndman, R.D., Currie, C.A., Mazzotti, S.P., 2005. Subduction zone backarcs, mobile belts, and orogenic heat. GSA Today 15, 4–10.

Jaupart, C., Mareschal, J.C., 1999. The thermal structure and thickness of continental roots. Lithos 48, 93–114.

Jordan, T.H., 1978. Composition and development of the continental tectosphere. Nature 274, 544–548.

Karato, S., 2003. Mapping water content in the upper mantle. In: Eiler, J. (Ed.), Inside the Subduction Factory. Geophysical Monograph, vol. 138. American Geophysical Union, Washington, DC, pp. 135–152.

Karato, S., Wu, P., 1993. Rheology of the upper mantle: a synthesis. Science 260, 771–778.

Kay, R.W., Kay, S.M., 1993. Delamination and delamination magmatism. Tectonophysics 219, 177–189.

Kincaid, C., Griffiths, R.W., 2003. Laboratory models of the thermal evolution of the mantle during rollback subduction. Nature 425, 58–62.
Lee, C., Yin, Q., Rudnick, R.L., Jacobsen, S.B., 2001. Preservation of ancient and fertile lithospheric mantle beneath the Southwestern United States. Nature 411, 69–73.
Lee, C.A., Lenardic, A., Cooper, C.M., Niu, F., Levander, A., 2005. The role of chemical boundary layers in regulating the thickness of continental and oceanic thermal boundary layers. Earth Planet. Sci. Lett. 230, 379–395.
Lowe, C., Ranalli, G., 1993. Density, temperature, and rheological models for the southeastern Canadian Cordillera: implications for its geodynamic evolution. Can. J. Earth Sci. 30, 77–93.
Mackwell, S.J., Zimmerman, M.E., Kohlstedt, D.L., 1998. High-temperature deformation of dry diabase with application to tectonics on Venus. J. Geophys. Res. 103, 975–984.
Molnar, P., Houseman, G.A., Conrad, C.P., 1998. Rayleigh–Taylor instability and convective thinning of mechanically thickened lithosphere: effects of non-linear viscosity decreasing exponentially with depth and of horizontal shortening of the layer. Geophys. J. Int. 133, 568–584.
Monger, J.W.H., Price, R.A., 2002. The Canadian Cordillera: geology and tectonic evolution. CSEG Recorder, pp. 17–36 (February).
Morency, C., Doin, M.P., 2004. Numerical simulations of the mantle lithosphere delamination. J. Geophys. Res. 109. doi:10.1029/2003JB002414.
Peslier, A.H., Reisberg, L., Ludden, J., Francis, D., 2000. Os isotopic systematics in mantle xenoliths: age constraints on the Canadian Cordillera lithosphere. Chem. Geol. 166, 85–101.
Pollack, H.N., 1986. Cratonization and thermal evolution of the mantle. Earth Planet. Sci. Lett. 80, 175–182.
Poudjom Djomani, Y.H., O'Reilly, S.Y., Griffin, W.L., Morgan, P., 2001. The density structure of subcontinental lithosphere through time. Earth Planet. Sci. Lett. 184, 605–621.
Pysklywec, R.N., Beaumont, C., 2004. Intraplate tectonics: Feedback between radioactive thermal weakening and crustal deformation driven by mantle lithosphere instabilities. Earth Planet. Sci. Lett. 221, 275–292.
Ranalli, G., Brown, R.L., Bosdachin, R., 1989. A geodynamic model for extension in the Shuswap core complex, southeastern Canadian Cordillera. Can. J. Earth Sci. 26, 1647–1653.
Rowland, A., Davies, J.H., 1999. Buoyancy rather than rheology controls the thickness of the overriding mechanical lithosphere at subduction zones. Geophys. Res. Lett. 26, 3037–3040.
Stegman, D.R., Freeman, J., Schellart, W.P., Moresi, L., May, D., 2006. Influence of trench width on subduction hinge retreat rates in 3-D models of slab rollback. Geochem. Geophys. Geosys. 7. doi:10.1029/2005/GC001056.
Stein, C.A., Stein, S., 1992. A model for the global variation in oceanic depth and heat flow with lithospheric age. Nature 359, 123–129.
Tao, W.C., O'Connell, R.J., 1992. Ablative subduction: a two-sided alternative to the conventional subduction model. J. Geophys. Res. 97, 8877–8904.
Thompson, A.B., 1992. Water in the Earth's upper mantle. Nature 358, 295–302.
van der Lee, S., Frederiksen, A., 2005. Surface wave tomography applied to the North American upper mantle. In: Levander, A., Nolet, G. (Eds.), Seismic Data Analysis and Imaging With Global and Local Arrays. Geophysical Monograph, vol. 157. American Geophysical Union, Washington DC, pp. 67–80.
van Hunen, J., Huang, J., Zhong, S., 2003. The effect of shearing on the onset and vigor of small-scale convection in a Newtonian rheology. Geophys. Res. Lett. 30. doi:10.1029/2003GL018101.
Willett, S.D., 1999. Rheological dependence of extension in wedge models of convergent orogens. Tectonophysics 305, 419–435.
Zelt, C.A., Ellis, R.M., Zelt, B.C., 2006. Three-dimensional structure across the Tintina strike–slip fault, northern Canadian Cordillera, from seismic refraction and reflection tomography. Geophys. J. Int. 167, 1292–1308.